LRP 392/90 January 1990

REVIEW OF FREE-ELECTRON-LASER (FEL) SIMULATION TECHNIQUES

T.M. Tran and J.S. Wurtele

Submitted for publication in
Computer Physics Reports

Review of Free-Electron-Laser(FEL) Simulation Techniques

T. M. Tran

Centre de Recherches en Physique des Plasmas
Association Euratom-Confédération Suisse
Ecole Polytechnique Fédérale de Lausanne

J. S. Wurtele

Department of Physics and the Plasma Fusion Center
Massachusetts Institute of Technology
Cambridge, Massachusetts 02139

In this paper, we review the techniques employed in the numerical simulations of free-electron-laser, in the amplifier as well as the oscillator configuration. Special emphases are given to the numerical problems associated with the particle initialization (particle loading), the treatment of the paraxial wave equation, the inclusion of oscillating space charge forces in the longitudinal particle motion and the multi-frequency modelling. This overview does not however include the particle-in-cell simulations commonly utilized in plasma physics: Due to the large scale between the wiggler and the radiation wavelength, this type of technique is impratical for short wavelength free-electron-laser.

Table of Contents

1. Introduction

One of the most noteworthy aspects of free electron laser (FEL) research continues to be the significant role of numerical simulation. From the development of the pendulum model of the FEL by Colson [1], and the subsequent [2] formulation relating the FEL equations to acceleration and particle trapping in an RF linac, numerical studies have been made to estimate gain, saturation amplitudes, efficiency enhancement, and the influence of beam energy spread and emittance. Simulation codes are widely used to compare experiment with theory and to design future experiments. They have also been employed to investigate theoretically predicted, but not yet experimentally observed, phenomena such as optical guiding.

Almost all experimental groups utilize simulation based on the nonlinear FEL equations for amplifier and oscillator systems. Depending on the experimental parameters, the nonlinear models need to be one-, two- or three-dimensional, with free space or waveguide boundary conditions. Amplifiers are often studied with single frequency simulations, but oscillators and amplifiers with sideband growth require multi-frequency simulations. Good agreement has been achieved between experiments and theory from UV to microwave frequencies.

The purpose of this paper is to provide a survey of FEL simulation techniques, with an emphasis on numerical problems particular to the FEL, e.g. the solution of the multi-dimensional paraxial wave equation, the inclusion of oscillating space-charge forces in the longitudinal particle motion, quiet particle loading, and multi-frequency modelling. A brief derivation of the well known equations for the FEL is presented in Sec. 2.

The FEL interaction will bunch the electron beam at the wavelength of the ponderomotive beat wave between the wiggler and radiation fields [$= (1/\lambda_w + 1/\lambda_s)^{-1}$, where λ_w is the wiggler wavelength, λ_s is the electromagnetic wavelength and $\lambda_s \approx \lambda_w/2\gamma_\parallel^2$ where $\gamma_\parallel^2 = 1/(1-\beta_\parallel^2)$]. The simplest FEL codes model amplifiers in which the beam is assumed to be periodic in the phase variable ψ, i.e., the phase of an electron in the ponderomotive wave. Particles are loaded between $\psi = -\pi$ and $\psi = \pi$,

corresponding to one representative ponderomotive wavelength of the beam. The "time" coordinate for the particle motion is usually the axial position z, not the time t. Thus the temporal structure of the electron beam is ignored in this approximation.

In the most straightforward one-dimensional approximation the wiggle motion is assumed to be identical for all particles, the transverse focusing of the beam from gradients in the wiggler and radiation fields, and all external focusing magnets, is neglected. The electromagnetic field is assumed to be a plane wave. In the tenuous beam (Compton) approximation, electrons interact with each other only indirectly, by coupling to the electromagnetic field through the source term in the wave equation. With only slight modification, however, the electrostatic forces from beam bunching can also be included. This inclusion of the electrostatic field is often needed for low electron beam energy and high current (Raman regime).

The utility of one-dimensional theory can be substantially improved by including the most important two-dimensional effects. Fill factors for the coupling of a finite radius electron beam to a waveguide mode or a diffracting Gaussian optical wave may be calculated analytically and included in a one dimensional theory. This reduces the coupling since some fraction of the wave power generated by the beam propagates outside the beam and, therefore, does not act back on it. The modification to the space-charge electrostatic wave resulting from conducting boundaries can also be handled by an appropriately calculated correction to the beam plasma frequency. The influence of emittance is modelled by an effective energy spread.

The details of more complicated multi-dimensional numerical simulations depend, of course, on the parameter regime of the system under study. For centimeter and millimeter wave experiments the beam often propagates in an overmoded waveguide, and can couple to many waveguide modes. In such cases, the conducting wall boundaries must be included in the analysis. This can be done either through a mode decomposition or by solving the wave equation with appropriate boundary conditions. At short wavelength ($< 100\mu$), the paraxial wave equation in free space must be solved with a two- or three-dimensional simulation. Transverse electron

orbits with betatron oscillations from the wiggler, external quadrupoles, and guide fields are readily studied by a separation of scales in which the fast wiggle oscillations are averaged over. Amplifier models are examined in Section 3.

When the temporal structure of a beam is important, or multi-frequency effects are investigated, the beam can no longer be assumed periodic in ψ with period 2π. The temporal structure of electron beams in an FEL depend on the accelerator that is used. RF linacs produce many short pulses of a few picoseconds each, while induction linacs produce pulses tens of nanoseconds long. The ponderomotive spatial scale is much shorter, in all but the longest wavelength experiments, than both the wiggler wavelength or the electron pulse length. More than one ponderomotive wavelength of the beam must be filled with particles, but it is impractical to fill each successive ponderomotive wavelength for an optical or infrared laser with a range of pulse lengths from picoseconds to nanoseconds. In addition, the wave amplitude varies in both z and t, and a partial differential equation must be solved.

The ability to use simulations to accurately predict frequency spectra in oscillators as a function of system parameters and optical and accelerator noise, cavity tuning and optical insertion devices (such as etalons) is of importance in the design of the next generation of FEL facilities [3]. The techniques associated with multi-frequency simulations are discussed in Section 4.

This paper does not treat one area of FEL simulations: those based on particle in cell plasma codes. Electromagnetic plasma codes have been examined in numerous texts and, because of the large separation of scales between the wiggler and optical wavelengths, are not practical for a short wavelength FEL. Our emphasis on numerical technique has allowed for little discussion of multiple waveguide mode modelling, which has been treated elsewhere [4,5].

2. Nonlinear Model of FEL

In this section, we derive the system of equations governing the motion of the individual electrons and the self-consistent evolution for the electromagnetic fields in a FEL. The particle equations of motion are obtained from a Hamiltonian formulation. The equations for the electromagnetic fields are derived from the Maxwell equations with the slowly varying amplitude and phase approximation. The electrostatic interaction between the electrons is then included by calculating the longitudinal electrostatic field of the bunched electrons and including this field in the energy evolution equation.

2.1. Single particle motion

For simplicity, we consider in this work only a circularly polarized magnetostatic wiggler. The resulting equations for other types of wigglers are formally very similar to those employed in this paper and can be found, for example in [1] for the linearly polarized magnetostatic wiggler and in [6] for the electromagnetic wiggler.

The circularly polarized wiggler and the induced electromagnetic field of the same polarization are characterized by the transverse vector potential $\vec{A}_\perp = (A_x, A_y)$, which can be written as :

$$A_x + iA_y = \frac{mc}{e}(a_x + ia_y) = -\frac{mc}{e}a_w e^{-ik_w z} + \frac{mc}{e}a_s e^{i(k_s z - \omega_s t + \phi_s)}, \qquad (2.1)$$

where $a_w = a_w(x,y,z)$ and $k_w = 2\pi/\lambda_w$ are the wiggler field amplitude and wave number, while $a_s = a_s(x,y,z,t)$, $\phi_s = \phi_s(x,y,z,t)$, k_s and ω_s are the transverse electromagnetic field's real amplitude, phase, wave number and frequency respectively. The complex amplitude $a_s e^{i\phi_s}$ is assumed to be a slowly varying function of the longitudinal coordinate z and the time t (eikonal approximation):

$$\left|\frac{\partial}{\partial z}\ln a_s e^{i\phi_s}\right| \ll k_s, \qquad \left|\frac{\partial}{\partial t}\ln a_s e^{i\phi_s}\right| \ll \omega_s. \qquad (2.2)$$

In the single frequency approximation, the quantities a_s, ϕ_s are independent of t.

Assuming that the electrostatic interactions between the electrons can be neglected, the equations of motion for a single electron are completely determined,

given the transverse potentials defined in (2.1). The Hamiltonian describing the motion of the particle through the wiggler can then be expressed in the following dimensionless form:

$$h(x,p_x,y,p_y,ct,-\gamma|z) = -\sqrt{\gamma^2 - 1 - p_x^2 - p_y^2 - a_x^2 - a_y^2 + 2(p_x a_x + p_y a_y)}. \quad (2.3)$$

Here, the canonical momenta (normalized to mc) p_x, p_y and the negative of the relativistic Lorentz factor γ, play the role of the momenta conjugate to the coordinates x, y, and ct respectively, with the space coordinate z being the independent variable [2], instead of the time t. In this case, the Hamiltonian h defined in (2.3) equals $-p_z$, where p_z is the longitudinal momentum in units of mc. The Hamiltonian equations are then:

$$\frac{d\vec{p}_\perp}{dz} = -\frac{\partial h}{\partial \vec{r}_\perp}, \quad \frac{d\vec{r}_\perp}{dz} = \frac{\partial h}{\partial \vec{p}_\perp}, \quad \frac{d(-\gamma)}{dz} = -\frac{\partial h}{\partial (ct)}, \quad \frac{d(ct)}{dz} = \frac{\partial h}{\partial (-\gamma)}, \quad (2.4)$$

where the '$\perp$' symbol designates the x, y transverse components. By taking an appropriate average of the Hamiltonian h over the wiggler period λ_w, the last term in parenthesis in (2.3) can be eliminated. Retaining only the first term in the expansion in $1/\gamma$ yields:

$$h(x,p_x,y,p_y,ct,-\gamma|z) = -\gamma + \frac{1 + |\vec{p}_\perp|^2 + |\vec{a}_\perp|^2}{2\gamma}. \quad (2.5)$$

From the expression for the vector potential given in (2.1),

$$|\vec{a}_\perp|^2 = a_w^2 + a_s^2 - 2a_w a_s \cos(\theta + \phi_s). \quad (2.6)$$

Here we have introduced the particle "phase" θ, defined by

$$\theta(z) = (k_w + k_s)z - \omega_s t(z). \quad (2.7)$$

In the case where only one wave frequency is present, the θ can replace the particle "coordinate" $t(z)$. From equations (2.4), the averaged motion of an electron in the

combined wiggler and electromagnetic fields is determined by the following first order equations:

$$\frac{d\vec{p}_\perp}{dz} = -\frac{1}{2\gamma}\frac{\partial |a_\perp|^2}{\partial \vec{r}_\perp}, \tag{2.8.a}$$

$$\frac{d\vec{r}_\perp}{dz} = \frac{\vec{p}_\perp}{\gamma}, \tag{2.8.b}$$

$$\frac{d\gamma}{dz} = -\frac{\omega_s}{\gamma c}\, a_w a_s \sin(\theta + \phi_s), \tag{2.8.c}$$

$$\frac{d\theta}{dz} = k_w - \frac{\omega_s}{c}\,\frac{1 + |p_\perp|^2 + a_w^2 + a_s^2 - 2a_w a_s \cos(\theta + \phi_s)}{2\gamma^2}, \tag{2.8.d}$$

$$\frac{d(ct)}{dz} = -\left[1 + \frac{1 + |p_\perp|^2 + a_w^2 + a_s^2 - 2a_w a_s \cos(\theta + \phi_s)}{2\gamma^2}\right]. \tag{2.8.e}$$

In the single frequency approximation, no t-dependence can be found on the right-hand side of the equations of motion, and thus the last equation (2.8.e) can be ignored. For time dependent or multiple frequency problems, the z-derivative is replaced by the convective derivative:

$$\frac{d}{dz} = \frac{\partial}{\partial z} + \frac{1}{c\beta_z}\frac{\partial}{\partial t} \tag{2.9}$$

in the Eqs.(2.8.a–d), with $1/\beta_z$ given by the RHS of (2.8.e).

In the one-dimensional approximation, all the electrons are assumed to be on ideal orbits with $\vec{p}_\perp = 0$. The influence of transverse beam temperature (emittance) is studied through an appropriately chosen energy spread. In this case, only the longitudinal equations (2.8.c–d) need to be considered, which results in the usual one-dimensional FEL equations [2]. The transverse equations (2.8.a,b) describe the betatron motion in the non-uniform wiggler and can be generalized to take into account any additional focusing field [7].

Until now, we have neglected the electrostatic interactions between the electrons; but in a low frequency FEL electrostatic effects are important (Raman regime operation). The above model may be extended to include space-charge effects by inserting a longitudinal electrostatic field into the γ equation (2.8.c), and omitting the

transverse electrostatic field as well as the transverse variations of the bunched electron beam density [8,9,10,11]. With these simplifications of the space-charge force, equation (2.8.c) is replaced by

$$\frac{d\gamma}{dz} = -\frac{\omega_s}{\gamma c} a_w a_s \sin(\theta + \phi_s) - \frac{eE_z}{mc^2}, \tag{2.10}$$

and the other equations of motion are unchanged. The self-consistent evolution of the transverse electromagnetic fields $a_s e^{i\phi_s}$, together with the longitudinal electrostatic field E_z, will be considered in the next subsection.

2.2. Field equations

The evolution of the transverse electromagnetic field and the longitudinal electrostatic field introduced above can be determined from the Maxwell equations, expressed in the Lorentz gauge:

$$\left(\nabla^2 - \frac{1}{c^2}\frac{\partial^2}{\partial t^2}\right)\vec{A} = -\mu_0 \vec{J}, \tag{2.11.a}$$

$$\left(\nabla^2 - \frac{1}{c^2}\frac{\partial^2}{\partial t^2}\right)\Phi = -\frac{\rho}{\epsilon_0}. \tag{2.11.b}$$

The transverse current can be constructed by adding the contributions from the N_p simulation particles, each carrying a charge $-q_j$:

$$J_x + iJ_y = -\sum_{j=1}^{N_p} q_j \frac{\beta_{xj} + i\beta_{yj}}{\beta_{zj}} \delta^2(\vec{r}_\perp - \vec{r}_{\perp j})\delta(t - t_j), \tag{2.12}$$

where $\vec{r}_{\perp j} = \vec{r}_{\perp j}(z)$ and $t_j = t_j(z)$ denote the trajectory of the particle j. The transverse velocities β_{xj}, β_{yj} can be related explicitly to the transverse canonical momenta p_{xj}, p_{yj} by

$$\gamma_j\beta_{xj} + i\gamma_j\beta_{yj} = -a_w e^{-ik_w z} + a_s e^{i(k_s z - i\omega_s t_j + \phi_s)} + p_{xj} + ip_{yj}. \tag{2.13}$$

The transverse complex field amplitude, as specified in (2.1), is determined by the transverse part of (2.11.a). Assuming the eikonal approximation (2.2), one can

write

$$\left[\nabla_\perp^2 + 2ik_s\left(\frac{\partial}{\partial z} + \frac{1}{v_g}\frac{\partial}{\partial t}\right)\right] a_s e^{i\phi_s} = -\frac{eZ_0}{mc^2}\left(J_x + iJ_y\right)e^{-i(k_s z - \omega_s t)}$$

$$= \frac{eZ_0}{mc^2}\sum_{j=1}^{N_p} q_j \frac{\beta_{xj} + i\beta_{yj}}{\beta_{zj}}\delta^2(\vec{r}_\perp - \vec{r}_{\perp j})\delta(t - t_j)e^{-i(k_s z - \omega_s t)}, \quad (2.14)$$

where v_g is the wave group velocity and $Z_0 = \mu_0 c$ is the impedance of free space.

In the single frequency steady state $\partial/\partial t = 0$, the equation (2.14) can be averaged over the wave period $2\pi/\omega_s$. Using (2.13) to eliminate the transverse velocities β_x, β_y yields:

$$\left[\nabla_\perp^2 + 2ik_s\frac{\partial}{\partial z}\right] a_s e^{i\phi_s} = -\frac{eZ_0 I}{mc^2}\left[\left\langle\frac{a_w e^{-i\theta}}{\gamma\beta_z}\right\rangle - \left\langle\frac{a_s e^{i\phi_s}}{\gamma\beta_z}\right\rangle\right], \quad (2.15)$$

where the particle phase θ has already been defined in (2.7), and the brackets denote a sum over the N_p particles, which each carry a partial current $I/N_p = \omega_s q_j/2\pi$, defined as follows:

$$\langle(\cdots)\rangle = \frac{1}{N_p}\sum_{j=1}^{N_p}\delta^2(\vec{r}_\perp - \vec{r}_{\perp j})(\cdots). \quad (2.16)$$

The betatron oscillation terms p_x, p_y in (2.13) have not contributed to (2.15), which is consistent with the averaging we performed to obtain the particle Hamiltonian in (2.5). Often the last term in the right-hand side of (2.15) is dropped, because $a_s \ll a_w$, and $\beta_z = 1$ is used for large γ. The field equation (2.15) is then reduced to the more familiar expression found in the literature [12,2,7].

The longitudinal wave equation for the electrostatic field $E_z = -\partial A_z/\partial t - \partial\Phi/\partial z$ can be readily obtained by combining the longitudinal part of (2.11.a) together with the equation (2.11.b) to yield:

$$\left(\nabla^2 - \frac{1}{c^2}\frac{\partial^2}{\partial t^2}\right)E_z = \frac{1}{\epsilon_0}\left[\frac{\partial\rho}{\partial z} + \frac{1}{c^2}\frac{\partial J_z}{\partial t}\right]. \quad (2.17)$$

The electrostatic field results from the charge bunching in the $\psi = \theta + \phi_s$ space as described in (2.8.d) and, therefore, can be assumed to be nearly periodic in this variable [8]. Thus, it can be expanded as a Fourier series:

$$E_z(x, y, z, t) = \sum_{l=-\infty}^{\infty} E_l(x, y, z)e^{il\psi}. \quad (2.18)$$

Note that $E_{-l} = E_l^*$ since E_z is real, so the expansion can be written as:

$$E_z(x,y,z,t) = \sum_{l=1}^{\infty} E_l(x,y,z)e^{il\psi} + \text{c.c.}, \tag{2.19}$$

where we have not treated the (nonresonant) D.C. space-charge component E_0. By taking the Fourier transform of (2.17), and assuming that E_l is slowly varying in z, one can obtain:

$$\left[\nabla_\perp^2 - \frac{l^2(k_w+k_s)^2}{\gamma_p^2}\right] E_l = \frac{il(k_w+k_s)}{\epsilon_0}\left[\rho_l - \frac{\beta_p}{c}J_l\right], \tag{2.20}$$

where $\beta_p = \omega_s/c(k_w+k_s) \simeq \beta_z$, $\gamma_p^2 = (1-\beta_p^2)^{-1} \simeq \gamma^2$, and ρ_l, J_l are the Fourier components of the density and the longitudinal current density respectively. Using the same representation for J_z as that for J_x, J_y defined in (2.12), and eliminating the charge density ρ_l with the help of the continuity equation (with the assumption that the transverse gradients of the space charge density ρ are small), the final form of the wave equation for E_z becomes:

$$\left[\nabla_\perp^2 - \kappa_l^2\right] E_l = -i\frac{Z_0 I}{\gamma_p}\kappa_l \left\langle e^{-il\psi}\right\rangle, \qquad \text{with} \quad \kappa_l \equiv \frac{l(k_w+k_s)}{\gamma_p}. \tag{2.21}$$

An approximate solution of (2.21) can be found by assuming that the electron beam is axisymmetric and uniform [11]. This yields:

$$E_z = \frac{2Z_0 I}{k_w+k_s}\sum_{l=1}^{\infty} f_l \frac{\langle \sin l\psi\rangle \cos l\psi - \langle \cos l\psi\rangle \sin l\psi}{l}, \tag{2.22}$$

where f_l is a space charge filling factor which depends on the beam radius r_b as:

$$f_l = 1 - \kappa_l r_b K_1(\kappa_l r_b), \tag{2.23}$$

where K_1 is the modified Bessel function of order one. With waveguide boundaries the factor f_l may have to be further modified to include reductions in the electrostatic field strength arising from nearby conducting walls.

Note that from the approximate solution (2.22) $\langle E_z\rangle = 0$; thus it is clear from (2.8.c) and (2.15) that the sum of the electromagnetic power

$$P_{\text{em}} = \left(\frac{mc^2}{e}\right)^2 \frac{1}{Z_0}\int\int k_s^2 a_s^2\, dxdy, \tag{2.24}$$

and the electron beam power

$$P_{\text{b}} = \frac{mc^2}{e} I\langle\gamma - 1\rangle \tag{2.25}$$

should be a constant of motion.

3. Single Frequency Simulations

The single frequency approximation in FEL simulations is, aside from its only modest requirement on computer resources, very important in the designs of FEL experiments. With this type of simulation code, extensive parametric analysis of FEL performances can be done, even with two-dimensional models [13,14]. It also provides a tool with which theoretical predictions can be checked, as has been done for the optical guiding phenomena [15,16].

For the single frequency model, the electromagnetic field amplitude a_s and phase ϕ_s do not depend on time t, and the FEL equations can be rewritten as:

$$\frac{d\vec{p}_\perp}{dz} = -\frac{1}{2\gamma}\frac{\partial a_w^2}{\partial \vec{r}_\perp}, \qquad \frac{d\vec{r}_\perp}{dz} = \frac{\vec{p}_\perp}{\gamma}, \tag{3.1.a}$$

$$\frac{d\gamma}{dz} = -\frac{\omega_s}{\gamma c} a_w a_s \sin(\theta+\phi_s) - 2\frac{eZ_0 I}{mc^2}\sum_{l=1}^{\infty} f_l \frac{\langle \sin l\psi\rangle \cos l\psi - \langle \cos l\psi\rangle \sin l\psi}{l(k_w+k_s)}, \tag{3.1.b}$$

$$\frac{d\theta}{dz} = k_w - \frac{\omega_s}{c}\frac{1+|p_\perp|^2+a_w^2-2a_w a_s\cos(\theta+\phi_s)}{2\gamma^2}, \tag{3.1.c}$$

$$\left[2ik_s\frac{\partial}{\partial z}+\nabla_\perp^2\right] a_s e^{i\phi_s} = -\frac{eZ_0 I}{mc^2}\left\langle \frac{a_w e^{-i\theta}}{\gamma}\right\rangle. \tag{3.1.d}$$

In these equations, we assume that $a_s \ll a_w$. To be complete, the above set of equations should be supplemented by both (a) the initial values of the particle phase space variables $(\psi, \gamma, \vec{r}_\perp, \vec{p}_\perp)$ at the wiggler entrance $z = 0$, (b) the initial electromagnetic field profile $a_s \exp(i\phi_s)$, and (c) the field boundary values in the transverse coordinates $\vec{r}_\perp$.

In the following, we will review successively the different methods for initializing the particle 6-dimensional distribution, the discretization of the transverse Laplacian operator $\nabla_\perp^2$, and the schemes to advance the particle variables and the electromagnetic field along the longitudinal coordinate z.

3.1. Particle loading

The most straightforward implementation of the initial particle distribution function $F(\psi, \gamma, \vec{r}_\perp, \vec{p}_\perp)$ is the use of a random number generator. For example, a uniform one-dimensional electron distribution $F(\psi, \gamma)$, is implemented with the following simple Fortran code segment:

```
      DO 100 IP=1,NPART
        PSI(IP) = PI * (2.*RANF()-1.)
        GAMMA(IP) = GAMMA0 + DELGAM*(2.*RANF()-1.)
100 CONTINUE
```

where NPART is the number of simulation particles and, RANF is the random number generator Fortran function (which may have a system dependent name). This method of particle loading has the obvious advantage of being very simple and working quite well in a low gain FEL as well as in the near-saturation regime (where the non-linear effects are very important), even with a modest number of simulation electrons (NPART ≤ 4000). It fails, however, when one tries to simulate the exponential growth in a high gain FEL fed with a very low initial (input) electromagnetic power. The reason for this failure is the relatively high noise level introduced by the random sampling of the initial particle phase space variables. In order to reduce these unwanted fluctuations introduced in the system, an excessive number of sampled particles might be required.

Another method of loading, which reduces the noise level, yet minimizes the correlations between the different sampled variables, uses the Hammersley's sequence, [17] defined as follows:

$$\{(j-1/2)/N, \Phi_2(j), \Phi_3(j), \Phi_5(j), \ldots, \Phi_r(j), \ldots\}, \qquad j = 1, \ldots, N. \tag{3.2}$$

In (3.2), $\Phi_r(j)$ is the radical inversion function in the base of a prime number r:

$$\Phi_r(j) = a_0 r^{-1} + a_1 r^{-2} + \cdots, \qquad j = a_0 + a_1 r^1 + \cdots \tag{3.3}$$

This yields, for example, the set [1/3, 2/3, 1/9, 1/3 + 1/9,...] when $r = 3$. This type of loader has been used to obtain quiet starts for particle-in-cell (PIC) plasma simulations [18].

An implementation of this in Fortran would consist of the following code segment, which calculates a set of NPART uniform values Y(J) in the interval $[0, 1]$:

```
      DO 100 J=1,NPART
        XS = 0.
        XSI = 1.0
        J2 = J
110     XSI = XSI/NBASE
        J1 = J2/NBASE
        XS = XS + (J2-NBASE*J1)*XSI
        J2 = J1
        IF( J2.GT.0 )  GOTO 110
100   Y(J) = XS
```

where NBASE is a prime number which corresponds to the base r of the radical inversion function Φ_r defined above.

The differences between these two methods of loading particles are illustrated in Fig.1a and Fig.1b. In the former, the 4096 values x_j, y_j are drawn from a random number generator, while in the latter, $x_j = (j - 1/2)/N$, $y_j = \Phi_2(j)$ with $N = 4096$. It is obvious that the distribution of x, y shown in Fig.1b is more uniform than that represented in Fig.1a, where localized bunching can be observed.

A quiet start method of particle loading was proposed in [15]. In this loader, only a small number (typically four) of particle phases ψ equally spaced in $[-\pi, \pi]$ are filled with identical particle distributions in the remaining variables $(\gamma, \vec{r}_\perp, \vec{p}_\perp)$; these distributions are sampled, using one of the two methods discussed above. This quiet start loader is particularly efficient for simulating the growth from a very low electromagnetic input power, in a high gain FEL ($G \gg 1$). The two other schemes generally fail in such circumstances.

One last particle initialization technique used in the waveguide FEL simulations [19] should be mentioned in this section. In this method, each of the initial particle space variables (ψ, r_0, θ_0) for a cylindrical beam is sampled using the N^{th} order Gaussian quadrature points with the appropriate weights. This is possible because, in the FEL model used in [19] (which is quite different from the one in this paper), the source terms of the field equations can be expressed in terms of integrals over (ψ, r_0, θ_0). For a cold beam (no spread in γ and $\vec{p}_\perp$), this technique already requires

1000 particles for a 10^{th} order Gaussian quadrature, hence it would be rather demanding of computer resources in a warm beam simulation. In addition, any desired phase-space distribution functions can be easily produced, using either the random sampling or Hammersley's sequences (see for example [17,18]), while it is not clear how to achieve this using this last technique of particle initialization.

3.2. Electromagnetic field calculations

The numerical treatment of the wave equation (3.1.d) and the scheme to interpolate the field values seen by the particles [Eqs.(3.1.b–c)] will be treated in this subsection. The methods that we shall present in detail are based on the use of a transverse spatial grid on which fields (a_s, ϕ_s) and various particle density functions ($\langle \sin l\psi \rangle$, $\langle \cos l\psi \rangle$, $\langle a_w \exp(-i\theta)/\gamma \rangle$) are defined. This approach is similar, in several aspects, to the PIC method used in plasma physics.

Integrating both members of Eq.(3.1.d) over a "volume" V, bounded by a closed "area" S, in the transverse space (x, y), and using the Green's identity and the definition of the brackets in (2.16), yields:

$$2ik_s \frac{d}{dz} \int_V \mathcal{A} dV + \int_S \vec{\nabla}_\perp \mathcal{A} \cdot d\vec{S} = -\frac{eZ_0}{mc^2} \frac{I}{N_p} \sum_{j \in \mathcal{J}} a_w(\vec{r}_{\perp j}) \frac{e^{-i\theta_j}}{\gamma_j}, \tag{3.4}$$

where $\mathcal{A}$ is the electromagnetic field complex amplitude $a_s \exp(i\phi_s)$ and $\mathcal{J}$ denotes all the particles that are located inside V.

Let us now specialize (3.4) to an axisymmetric electromagnetic field. Divide the radial axis into N_r intervals bounded by $r_{k+1/2}$, $k = 0, 1, \ldots, N_r$, with $r_{1/2} = 0$ and $r_{N_r+1/2} = R_{\max}$. The intervals $[r_{k-1/2}, r_{k+1/2}]$ need not be equal, and the value of $R_{\max}$ is chosen to be much larger than both the electron beam size and the initial electromagnetic beam radius. Hence, the "volume" V_k and the "area" $S_{k+1/2}$ introduced in Eq.(3.4) can be expressed as:

$$V_k = \pi(r_{k+1/2}^2 - r_{k-1/2}^2), \qquad S_{k+1/2} = 2\pi r_{k+1/2}. \tag{3.5}$$

Defining the grid values $\mathcal{A}_k(z) = \mathcal{A}(r_k, z)$ where $r_k = (r_{k-1/2} + r_{k+1/2})/2$ is the mid-point of the interval $[r_{k-1/2}, r_{k+1/2}]$, the first and second terms of the left-hand side of Eq.(3.4) can be approximated in terms of the grid quantities as

$$2ik_s \frac{d}{dz} 2\pi \int_{r_{k-1/2}}^{r_{k+1/2}} \mathcal{A} r dr \simeq 2ik_s V_k \frac{d\mathcal{A}_k}{dz} \tag{3.6}$$

and

$$\int_{S_k} \vec{\nabla}_\perp \mathcal{A} \cdot d\vec{S} \simeq S_{k+1/2} \frac{\mathcal{A}_{k+1} - \mathcal{A}_k}{r_{k+1} - r_k} - S_{k-1/2} \frac{\mathcal{A}_k - \mathcal{A}_{k-1}}{r_k - r_{k-1}} \tag{3.7}$$

respectively. In (3.6), the grid value $\mathcal{A}_k$ is approximated by an average of $\mathcal{A}$ over the interval k, and, in (3.7), the first order finite differences have been used to discretize the radial derivative.

Substitution of Eqs (3.6) and (3.7) into Eq.(3.4) yields a set of N_r ordinary differential equations for $\mathcal{A}_k(z)$:

$$\begin{aligned} \frac{d\mathcal{A}_k}{dz} = & \frac{i}{2k_s} \sum_{k'=1}^{N_r} M_{k,k'} \mathcal{A}_{k'} \\ & + \frac{i}{V_k} \frac{eZ_0}{mc^2} \frac{1}{2k_s} \frac{I}{N_p} \sum_{j \in \mathcal{J}_k} a_w(\vec{r}_{\perp j}) \frac{e^{-i\theta_j}}{\gamma_j}, \qquad k = 1, \ldots, N_r, \end{aligned} \tag{3.8}$$

where $M_{k,k'}$ is a real tridiagonal finite difference matrix:

$$M_{k,k-1} = \frac{1}{V_k} \frac{S_{k-1/2}}{r_k - r_{k-1}}, \quad M_{k,k+1} = \frac{1}{V_k} \frac{S_{k+1/2}}{r_{k+1} - r_k}, \quad M_{k,k} = -M_{k,k-1} - M_{k,k+1}. \tag{3.9}$$

The boundary conditions, at $r = R_{\max}$, on $\mathcal{A}$ are enforced either (a) by setting $M_{N_r,N_r+1} = 0$ in the case of the natural boundary condition $r\partial\mathcal{A}/\partial r = 0$ (as can be deduced from (3.7)), or (b) simply by setting $\mathcal{A}_{N_r+1} = 0$ in Eq. (3.8) in the case of the essential boundary condition $\mathcal{A} = 0$.

It should be noted that the second term in (3.8), which is proportional to the current density of the bunched electrons, can be viewed as a "nearest grid point" (NGP) charge assignment employed in PIC simulations. In other words, the particle density is approximated by a piecewise constant function on the interval $[r_{k-1/2}, r_{k+1/2}]$, as is the electromagnetic field (see Eq. (3.6)). Consistent with this, the electromagnetic field $\mathcal{A}$ and the electrostatic field seen by an electron located in the interval

$[r_{k-1/2}, r_{k+1/2}]$ should both be approximated by their respective grid quantities: For the electromagnetic field, it is just the solution $\mathcal{A}_k$ of (3.8), while for the electrostatic field, which is proportional to the second term of the right-hand side of (3.1.b), the following relation can be used:

$$\langle \sin l\psi \rangle + i\langle \cos l\psi \rangle \simeq \frac{2\pi}{V_k} \int_{r_{k-1/2}}^{r_{k+1/2}} \langle e^{il\psi} \rangle \, r dr = \frac{1}{V_k N_p} \sum_{j \in \mathcal{J}_k} e^{il\psi_j}. \tag{3.10}$$

It can be shown that the balance between the electron beam power defined in (2.25) and the electromagnetic power written in terms of the grid values as:

$$\frac{m^2 c^4}{e^2 Z_0} \sum_{k=1}^{N_r} V_k |k_s \mathcal{A}_k|^2 \tag{3.11}$$

is exactly preserved in the numerical model when the charge assignment and the field interpolation scheme described above are employed [12]. This conservation property is a very useful diagnostic tool for the simulation code.

The finite difference method presented here can be extended to the two-dimensional Cartesian case, starting from the wave equation (3.4). It has been considered in [20], using a five-point finite difference to approximate the Laplacian in Eq.(3.7).

3.3. Higher order schemes

Higher order charge assignment and interpolation schemes can, at least in principle, be constructed in a straightforward manner. One method is to start from the *weak variational form* [21] of the electromagnetic equation which can be derived by multiplying Eq.(3.1.d) by a *test function* $\mathcal{G}(\vec{r}_\perp)$ and integrating it on the whole transverse space domain. Applying the Green's identity would then yield

$$2ik_s \frac{d}{dz} \int \mathcal{A}\mathcal{G} \, d^2\vec{r}_\perp - \int \vec{\nabla}_\perp \mathcal{A} \cdot \vec{\nabla}_\perp \mathcal{G} \, d^2\vec{r}_\perp = -\frac{eZ_0}{mc^2} \frac{I}{N_p} \sum_{j=1}^{N_p} a_w(\vec{r}_{\perp j}) \frac{e^{-i\theta_j}}{\gamma_j} \mathcal{G}(\vec{r}_{\perp j}). \tag{3.12}$$

The problem of solving for the field amplitude $\mathcal{A}$ can then be stated as follows: For all "sufficiently smooth" test functions $\mathcal{G}(\vec{r}_\perp)$, find the field $\mathcal{A}$ such that the integral equation defined in (3.12) is verified. The technique to solve this variational problem, using the finite elements method numerically, can best be illustrated by considering

the axisymmetric case. First, the interval $[0, R_{\max}]$ (with $R_{\max}$ sufficiently large such that the electromagnetic field is negligible at r larger than $R_{\max}$), is cut into N_r sub-intervals (or elements) $[r_{k-1}, r_k]$, $k = 1, \ldots, N_r$. Assuming that the solution $\mathcal{A}$ is *linear* on each of these intervals leads to the following formulation for $\mathcal{A}$:

$$\mathcal{A}(r,z) = \sum_{k=0}^{N_r-1} \mathcal{A}_k(z)\Lambda_k(r), \tag{3.13}$$

where $\mathcal{A}_k(z) = \mathcal{A}(r_k, z)$ and the real function $\Lambda_k(r)$ is the "hat function" which is zero outside the interval $[r_{k-1}, r_{k+1}]$ and piecewise linear inside this interval, as shown in Fig.(2).

Inserting the expansion defined in (3.13) into the weak form (3.12) and using the linear basis functions $\Lambda_k(r)$ as test functions yields a system of N_r ordinary differential equations for $\mathcal{A}_k(z)$:

$$\begin{aligned} 2ik_s \sum_{k'=0}^{N_r-1} P_{k,k'} \frac{d\mathcal{A}_{k'}}{dz} = \sum_{k'=0}^{N_r-1} M_{k,k'}\, \mathcal{A}_{k'} \\ - \frac{eZ_0}{mc^2} \frac{I}{N_p} \sum_{j=1}^{N_p} a_w(r_j) \frac{e^{-i\theta_j}}{\gamma_j} \Lambda_k(r_j), \quad k = 0, \ldots, N_r - 1, \end{aligned} \tag{3.14}$$

where the matrices $P_{k,k'}$ and $M_{k,k'}$ can be calculated analytically from the following integrals:

$$\begin{aligned} P_{k,k'} &= 2\pi \int \Lambda_k(r)\Lambda_{k'}(r) r\, dr, \\ M_{k,k'} &= 2\pi \int \Lambda'_k(r)\Lambda'_{k'}(r) r\, dr. \end{aligned} \tag{3.15}$$

Note that the matrices $P_{k,k'}$, $M_{k,k'}$ are tridiagonal, the hat functions $\Lambda_k(r)$ being non-zero only in two adjacent intervals [see Fig.(2)]. Note, also, that in the second term of the right hand side of (3.14), only particles located in $[r_{k-1}, r_{k+1}]$ are taken into account with their appropriate weight $\Lambda_k(r_j)$.

The expansion (3.13) should be used, for consistency, for the expression of the electromagnetic field $\mathcal{A}$ in the particle equations. It enables us to evaluate the field $\mathcal{A}$ at any particle radial position. Similarly, the same expansion can be applied to

the electrostatic terms $\langle \cos l\psi \rangle$, $\langle \sin l\psi \rangle$ as follows:

$$\langle e^{il\psi} \rangle (r,z) = \sum_{k=0}^{N_r-1} \langle e^{il\psi} \rangle_k (z) \Lambda_k (r), \tag{3.16}$$

where the grid values $\langle e^{il\psi} \rangle_k$ are computed by inverting the following tridiagonal system of equations numerically:

$$\sum_{k'=0}^{N_r-1} P_{k,k'} \langle e^{il\psi} \rangle_{k'} = \frac{1}{N_p} \sum_{j=1}^{N_p} e^{il\psi_j} \Lambda_k (r_j), \quad k = 0, \ldots, N_r - 1. \tag{3.17}$$

The expansion using the linear finite elements as described above, is similar to the first-order weighting cloud-in-cell (CIC) scheme employed in plasma physics. Starting from the weak variational form (3.12), higher-order expansions (quadratic elements, cubic splines etc.) can be derived in a systematic manner, by choosing the appropriate basis functions.

It is worth mentioning other approaches that use *global* functions as basis functions in the expansion (3.13) instead of the *local* functions considered above. In Ref.[22], eigenfunctions of the wave function (3.1.d) are used in the expansion: Gaussian-Hermite polynomials in the Cartesian (x, y) representation, and Gaussian-Laguerre polynomials for an axisymmetric FEL configuration. In closed waveguide FEL configurations in which the full Maxwell equations should be considered instead of the scalar wave equation (3.1.d), expansions using the TE, TM waveguide eigenmodes are generally used (see for example [4,5,23]). In general, these methods are restricted to problems which require expansions with only a few modes, because of the computational cost in evaluating the complicated basis functions. According to Ref.[22], the cost of computation is spent mainly on the electromagnetic field calculations, in contrast with the grid methods in which the CPU time needed to solve the discretized wave equations (3.8) or (3.14) is much less than that spent in advancing the particles [12]. In order to reduce the number of terms kept in the expansion, variants of these spectral methods have been introduced [24, 25]. The thrust of these methods is to introduce appropriate free parameters into the expansions. They can

be very accurate, even with a relatively few number of modes, provided that the free parameters have been chosen well.

3.4. Integration along the longitudinal direction

The treatment of the Laplacian in the wave equation, using either the finite differences, the finite elements or the spectral methods discussed above, results in a system of $2N_r$ real first order ordinary differential equations for the grid values (or expansion terms in spectral methods) of the electromagnetic field. Together with the particle equations (3.1.a–c), they form a set of $6N_p + 2N_r$ ODEs in the most general case, in which the transverse betatron motion is taken into account.

One way to solve this system of ODEs is to integrate the whole system *simultaneously* using, for instance, the Runge-Kutta method, which is very easy to implement. More sophisticated integrators have been tried, such as the Gear predictor-corrector method [26]. These latter types of integrators, which can be found in many numerical libraries, are, however, very costly in both computer storage and CPU time. For example, the `DGEAR` routine found in the `IMSL` library [27] requires a working array whose dimension is seventeen times the number of ODEs! In the spectral methods which require a few modes to represent the electromagnetic field accurately, this is still affordable. In cases where a large number of grid values for the field (which in turn requires a large number of simulation particles to generate a smooth representation of the electron current density), simple schemes are mandatory, specially in the fully three dimensional codes.

A simple scheme has been proposed in Ref.[12]. In this scheme, the integration of the $6N_p$ particle equations is performed by a special low storage fourth order Runge-Kutta algorithm developed by Blum [18, 28]. The field equations (3.14), which are already an approximation of the original wave equation, require only a less accurate treatment than that used for the particle equations. Using the first order forward difference to approximate the z-derivative, the field equations (3.14) can then be put in the following matrix form:

$$\left[\mathbf{P} + i\frac{\Delta z}{4k_s}\mathbf{M}\right]\mathbf{a}(z+\Delta z) = \left[\mathbf{P} - i\frac{\Delta z}{4k_s}\mathbf{M}\right]\mathbf{a}(z) - i\frac{\Delta z}{4k_s}\mathbf{s}(z-\Delta z/2) \qquad (3.18)$$

where the array **s** represents the second term of the right-hand side of Eq.(3.14). Since the matrices **P**, **M** are tridiagonal in the axisymmetric case, a very fast direct Gauss elimination can be performed to solve (3.18). Using, then, the solution $\mathbf{a}(z + \Delta z)$, the particle equations can be advanced from $z - \Delta z/2$ to $z + \Delta z/2$, followed by the construction of the new source **s** from the particle variables defined now at $z + \Delta z/2$. In this way, the centering in z of the wave equation discretization is preserved. This algorithm for marching in z is analogous to the usual *leapfrog* time stepping algorithm. In two-dimensional Cartesian coordinates, the iterative ADI (Alternating Direction Implicit) method has been employed [20], although direct elimination can still be done, since the matrices are sparse.

4. Time Dependent Simulations

Thus far, we have assumed that the electromagnetic field $a_s \exp(i\phi_s)$ is time independent, i.e. only a single frequency is present in the system. In the time dependent case, the source term for the wave equation (2.14) is no longer constant in time. The resulting non-uniform gain deposition along the electromagnetic pulse during the FEL interaction can induce a modulation in the wave amplitude $a_s \exp(i\phi_s)$ and excite a multimode (or sideband) spectrum. This effect was pointed out in Ref.[2], where it was discussed for a tapered wiggler FEL. Sideband growth can cause particles to be detrapped from the ponderomotive potential, thereby lowering the FEL efficiency. The instability can occur even in an untapered wiggler configuration [29,30], because of the strongly overmoded resonators employed in FEL oscillators. A transition to a stochastic regime may take place in the case of strong instability [31,32]. Furthermore, one has to take into account the difference between the axial electron velocity v_z and the electromagnetic pulse velocity v_g. A a result of this difference, the electrons slip behind the electromagnetic pulse along their transit through the wiggler whose length is L, by

$$s = L\,(1/v_z - 1/v_g)\,, \tag{4.1}$$

called the *slippage* time, which is of the order of $2\pi N/\omega_s = N\lambda_s/c$ for electrons close to the resonance, N being the number of wiggler periods. Notice that this slippage is much smaller than the wave transit time L/v_g through the wiggler, but much larger than the wave period. When the electron pulse duration is short ($t_p \sim s$), the non-uniform gain deposition results in *laser lethargy*, first analyzed in Ref.[33]. The analysis of this effect was refined in Refs.[34,35].

4.1. Mathematical formulation

In the following discussion, we will concentrate on the techniques used in the simulation of the time dependent effects and discard, for simplicity, the transverse spatial non-uniformities (wave diffraction and betatron motion) already discussed in detail in the previous section, as well as the space-charge electric field. Consider an n^{th} pass through the resonator whose length is L_r. Denoting the electromagnetic field amplitude during this pass by $\mathcal{A}^{(n)} = a_s^{(n)} \exp(i\phi_s^{(n)})$ and expressing the particle equations (2.8.c–e) and the wave equation (2.14) in the characteristic variable for the wave (or particle retarded time)

$$t' = t - z/v_g, \tag{4.2}$$

yields the following one dimensional time dependent equations:

$$\frac{d\gamma_j}{dz} = -\frac{\omega_s}{\gamma_j c}\, a_w a_s^{(n)} \sin(\theta_j + \phi_s^{(n)}), \tag{4.3.a}$$

$$\frac{d\theta_j}{dz} = k_w - \frac{\omega_s}{c}\,\frac{1 + a_w^2 - 2a_w a_s^{(n)} \cos(\theta_j + \phi_s^{(n)})}{2\gamma_j^2}, \tag{4.3.b}$$

$$\frac{d(ct'_j)}{dz} = \frac{1}{\beta_{zj}} - \frac{c}{v_g} = \frac{c}{L} s_j = \left(1 - \frac{c}{v_g}\right) + \frac{1 + a_w^2 - 2a_w a_s^{(n)} \cos(\theta_j + \phi_s^{(n)})}{2\gamma_j^2}, \tag{4.3.c}$$

$$2ik_s \frac{\partial}{\partial z}\mathcal{A}^{(n)}(t', z) = -\frac{eZ_0}{mc^2}\frac{Q}{A_b N_p}\sum_{j=1}^{N_p} \delta(t' - t'_j)\frac{a_w e^{-i\theta_j}}{\gamma_j}. \tag{4.3.d}$$

In (4.3.d), we assume that each electron j carries a charge density $Q/A_b N_p$, where Q and A_b are, respectively, the total charge and the cross-section of the electron pulse injected into the wiggler. The initial conditions for the N_p electrons can be specified by a particle distribution function $F(\gamma, \theta, t')$ defined at the entrance of the wiggler

$z = 0$ and *at each pass* n. The beam distribution in t' is defined in the interval $[0, t_p]$ for an electron pulse of duration t_p. The limiting case of a continuously injected electron beam would have to be modeled with $-\infty < t' < \infty$. However, since the electromagnetic field $\mathcal{A}^{(n)}$ is periodic in t',

$$\mathcal{A}^{(n)}(t' + T_r, z) = \mathcal{A}^{(n)}(t', z), \qquad T_r \equiv 2L_r/c, \tag{4.4}$$

only the interval $[0, T_r]$ must be considered. In practice, some long pulse simulations employ a small "window" (of the order of a few slippage times s) in t' [32] in order to cut down the computational cost, but this is done at the expense of lower resolution in the Fourier spectrum for the electromagnetic field.

For the wave equation (4.3.d), one should define an initial electromagnetic pulse shape $\mathcal{A}(t', z = 0)$ for the first pass. In the following passes, the boundary condition

$$\mathcal{A}^{(n)}(t', z = 0) = R\mathcal{A}^{(n-1)}(t', z = L), \tag{4.5}$$

where R is the complex reflectivity of the resonator mirrors, provides the initial condition required to integrate the wave equation (4.3.d). The numerical methods needed to solve the system of equations (4.3), together with the particle and wave initial conditions discussed above are treated in the next subsections.

4.2. Discretization of the time dependent equations

In comparing the source term of the wave equation (4.3.d) with that found in the single frequency two-dimensional model, Eq.(3.1.d), it is worth noting that the wave variable t' plays a role which is very similar to that of the radial coordinate r. Using this analogy, one can then discretize the electromagnetic field amplitude $\mathcal{A}^{(n)}$, with a "temporal grid" on which the grid quantities

$$\mathcal{A}_k^{(n)}(z) \equiv \mathcal{A}^{(n)}(t' = t'_k, z) \tag{4.6}$$

are defined. Integrating the Eq.(4.3.d) over the interval $[t'_{k-1/2}, t'_{k+1/2}]$ yields the following set of first order ODEs:

$$\Delta t'_k \frac{d\mathcal{A}_k^{(n)}}{dz} = \frac{i}{2k_s} \frac{eZ_0}{mc^2} \frac{Q}{A_b N_p} \sum_{j \in \mathcal{J}_k} \frac{a_w e^{-i\theta_j}}{\gamma_j}, \quad k = 1, \ldots N_t \tag{4.7}$$

where $\Delta t'_k = t'_{k-1/2} - t'_{k+1/2}$ and $\mathcal{J}_k$ denotes those particles having their retarded time t' inside the interval $[t'_{k-1/2}, t'_{k+1/2}]$. This field discretization is nothing but the NGP charge assignment scheme described in section 3.2. The electromagnetic field $\mathcal{A}^{(n)}$ seen by the particles can then be interpolated, following the same NGP method.

This system of ODEs for the electromagnetic wave, together with the $3N_p$ particle equations (4.3.a–c) may then be integrated, *for each pass* through the wiggler, using one of the marching schemes presented in section 3.4. The whole multiple pass procedure can now be summarized as follows:

a. Initialize the electromagnetic field profile $\mathcal{A}^{(0)}(t', 0)$.

b. Initialize the particle variables γ, θ and t', using one of the sampling methods described in section 3.1.

c. Advance the particles as well as the electromagnetic field toward the exit of the wiggler $z = L$, by integrating the system of particle equations (4.3.a–c) and wave equations (4.7).

d. Set the electromagnetic field profile at the entrance of the wiggler $z = 0$ as prescribed by the boundary condition (4.5). The next pass calculation, starting with step b., can then be performed.

It should be noted that the higher order schemes cited in section 3.3 can be applied to discretize the t' variable as well. In addition, since the field amplitude is periodical as stated in Eq.(4.4), the Fourier transform method could be used. Defining an equally spaced grid $t'_k = kT_r/N_r$, $k = 0, \ldots, N_r - 1$, the finite discrete Fourier transform of $\mathcal{A}^{(n)}(t')$ is then:

$$\tilde{\mathcal{A}}_l^{(n)} = \frac{1}{N_r} \sum_{k=0}^{N_r-1} \mathcal{A}^{(n)}(t'_k) \exp(-\frac{2\pi i}{N_r} kl). \tag{4.8}$$

The inverse transform is:

$$\mathcal{A}^{(n)}(t'_k) = \sum_{l=-N_r/2}^{N_r/2} \tilde{\mathcal{A}}_l^{(n)} \exp(\frac{2\pi i}{N_r} kl). \tag{4.9}$$

The ODEs for $\mathcal{A}_l^{(n)}$ are obtained by taking the Fourier transforms of Eq.(4.3.d):

$$\frac{d\tilde{\mathcal{A}}_l^{(n)}}{dz} = \frac{i}{2k_s}\frac{eZ_0}{mc^2}\frac{Q}{A_b N_p}\frac{1}{T_r}\sum_{j=1}^{N_p}\frac{a_w e^{-i(\theta_j + 2\pi l t_j'/T_r)}}{\gamma_j}, \quad l = -N_r/2, \ldots N_r/2, \quad (4.10)$$

while the field seen by the particles is interpolated from the grid values given in (4.9), using either the NGP scheme or higher order ones. The merit of this method is that the FFT algorithm used to compute the sum (4.9) is very fast. Using a small window $w \ll T_r$ [32] can further reduce the overall computational time.

4.3. Low gain approximation

The multiple pass method as described in the previous subsection can be very time consuming in a low gain FEL because of the large number of passes required to reach the saturation. When low gain and high mirror reflectivity ($|R| \simeq 1$) hold, an approximated wave equation [31,36] can be derived. First integrate Eq.(4.3.d) over the wiggler length, taking into account the boundary condition (4.5), to find:

$$\mathcal{A}^{(n+1)}(t',0) - \mathcal{A}^{(n)}(t',0) + (1-R)\mathcal{A}^{(n)}(t',0) = \frac{iR}{2k_s}\frac{eZ_0}{mc^2}\frac{Q}{A_b N_p}\int_0^L dz \sum_{j=1}^{N_p}\delta(t'-t_j')\frac{a_w e^{-i\theta_j}}{\gamma_j}. \quad (4.11)$$

Making the assumptions of low gain, $|R| \simeq 1$, and

$$\left|\frac{\mathcal{A}^{(n+1)}(t',0) - \mathcal{A}^{(n)}(t',0)}{\mathcal{A}^{(n)}(t',0)}\right| \ll 1, \quad (4.12)$$

allows us to introduce a continuous slow time $\tau = 2nL_r/v_g$, which can replace the discrete pass number n. Thus, the approximated field amplitude is constant in z, can be written as $\mathcal{A} = \mathcal{A}(\tau, t')$, and satisfies the partial differential equation:

$$\left[\frac{\partial}{\partial\tau} + (1-R)\frac{v_g}{2L_r}\right]\mathcal{A}(\tau,t') = \frac{i}{2k_s}\frac{v_g}{2L_r}\frac{eZ_0}{mc^2}\frac{Q}{A_b N_p}\int_0^L dz\sum_{j=1}^{N_p}\delta(t'-t_j')\frac{a_w e^{-i\theta_j}}{\gamma_j}. \quad (4.13)$$

The virtue of this formulation is in its providing the possibility of reaching the saturation in the low gain FEL oscillator rapidly. This is accomplished by using implicit time (in the slow time τ) schemes that allow time steps much larger than T_r (see for example [37]). Thus far, this type of simulation has not, to our knowledge, been explored.

5. Conclusion

In this paper we have presented a survey of techniques for FEL simulations. Particular emphasis has been placed on the development of multi-dimensional FEL codes in free space and the time-dependent simulations. Numerical models have been quite successful in predicting the gain and phase shift of the FEL in the linear and nonlinear regimes. Simulations have been developed for a large number of experiments, from the centimeter to visible wavelengths, and may have an even more important part in the design of the next generation of FEL facilities.

References

[1] W. B. Colson, IEEE J. Quantum Electron. 17 (1981) 1417

[2] W. M. Kroll, P. L. Morton and M. W. Rosenbluth, IEEE J. Quantum Electron. 17 (1981) 1436.

[3] P. W. Van Amersfoort, R. W. B. Best, B. Faatz, C. A. J. Van der Geer, W. J. Mastop, B. J. H. Meedens, A. F. G. Van der Meer, D. Oepts and M. J. Van der Wiel, in Proc. of the 10th Int. FEL Conf., Jerusalem (1988), to be published.

[4] J. S. Wurtele, E. T. Scharlemann, and A. M. Sessler, Nucl. Instr. Methods Phys. Res. A250 (1986) 176.

[5] J. Beyers, Nucl. Instr. Methods Phys. Res. A272 (1988) 590.

[6] T. M. Tran, B. G. Danly and J. S. Wurtele, IEEE J. Quantum Electron. 23 (1987) 1578.

[7] E. T. Scharlemann, J. Appl. Phys. 58 (1985) 2154.

[8] D. Protsnitz, A. Szoke and V. K. Neil, Phys. Rev. A24 (1981) 1436.

[9] C. M. Tang and P. A. Sprangle, J. Appl. Phys. 52 (1981) 3148.

[10] A. K. Ganguly and H. P. Freund, Phys. Fluids 31 (1988) 387.

[11] T. J. Orzechowski, E. T. Scharlemann, B. Anderson, V. K. Neil, W. M. Fawley, D. Prosnitz, S. M. Yarema, D. B. Hopkins, A. C. Paul, A. M. Sessler, and J. S. Wurtele, IEEE J. Quantum Electron. 21 (1985) 831.

[12] T. M. Tran and J. S. Wurtele, Comp. Phys. Commun. 54 (1989) 263.

[13] J. .E. LaSala, D. A. G. Deacon and J. M. J. Madey, Nucl. Instr. Methods Phys. Res. A250 (1986) 262.

[14] R. A. Jong and E. T. Scharlemann, Nucl. Instr. Methods Phys. Res. A259 (1987) 254.

[15] J. E. LaSala, D. A. G. Deacon, and E. T. Scharlemann, Nucl. Instr. Methods Phys. Res. A250 (1986) 389.

[16] E. T. Scharlemann, LLNL Preprint UCRL 96329 (1987).

[17] J. M. Hammersley and D. C. Handscomb, *Monte Carlo Methods*, Methuen, London, (1964).

[18] C. K. Birdsall and A. B. Langdon, *Plasma Physics via Computer Simulations*, McGraw-Hill, New-York (1985).

[19] A. K. Ganguly and H. P. Freund, Phys. Rev. A32 (1985) 2275.

[20] B. D. McVey, Nucl. Instr. Methods Phys. Res. A250 (1986) 449.

[21] G. Strang and G. J. Fix, *An Analysis of the Finite Element Method*, Prentice-Hall, Englewoods Cliffs (1973).

[22] C. M. Tang and P. A. Sprangle, IEEE J. Quantum Electron. 21 (1985) 970.

[23] H. P. Freund, H. Bluem and C. L. Chang, Phys. Rev. A36 (1987) 2182.

[24] P. Sprangle, A. Ting and C. M. Tang, Nucl. Instr. Methods Phys. Res. A259 (1987) 136.

[25] G. Bourianof, B. Moore, M. Rosenbluth, F. Waelbroeck, H. Waelbroeck and H. G. Wong, Nucl. Instr. Methods Phys. Res. A272 (1988) 340.

[26] W. M. Fawley, D. Prosnitz and E. .T. Scharlemann, Phys. Rev. A30 (1984) 2472.

[27] IMSL Library, User's Manual, ed.9.2, Houston, TX (1984).

[28] E. K. Blum, *Math. Comp.*, **16** (1962) 176.

[29] J. C. Goldstein and W. B. Colson, Proc. of the Int. Conf on Lasers 82 (1982) 218.

[30] W. B. Colson and R. A. Freedman, Opt. Commun. 46 (1983) 37

[31] Y. L. Bogomolov, V. L. Bratman, N. S. Ginzburg, M. I. Petelin and A. D. Yunakovsky, Opt. Commun. 36 (1981) 209

[32] W. B. Colson, in Free Electron Generators of Coherent Radiation, SPIE Vol. 453, Proc. Soc. Photo-Opt. Instr, Eng. (1984) 289

[33] H. Al-Abawi, F. A. Hopf, G. T. Moore and M. O. Scully, Opt. Commun. 30 (1979) 235.

[34] W. B. Colson and S. K. Ride, in Physics of Quantum Electronics, Vol. 7, Addison-Wesley Reading, Mass. (1980) 377.

[35] P. Sprangle, C. M. Tang and I. Bernstein Phys. Rev. A28 (1983) 2300.

[36] N. S. Ginzburg and M. I. Petelin, Int. J. Electron. 59 (1985) 291.

[37] T. Tajima, *Computational Plasma Physics: With Applications to Fusion and Astrophysics*, Addison-Wesley, (1989).

Figure Captions

Fig. 1 The x and y phase space variables sampled, using (a) a random number generator and (b) using the Hammersley's sequence. The number of points N is 4096.

Fig. 2 The piecewise linear "hat" functions $\Lambda_k(r)$.

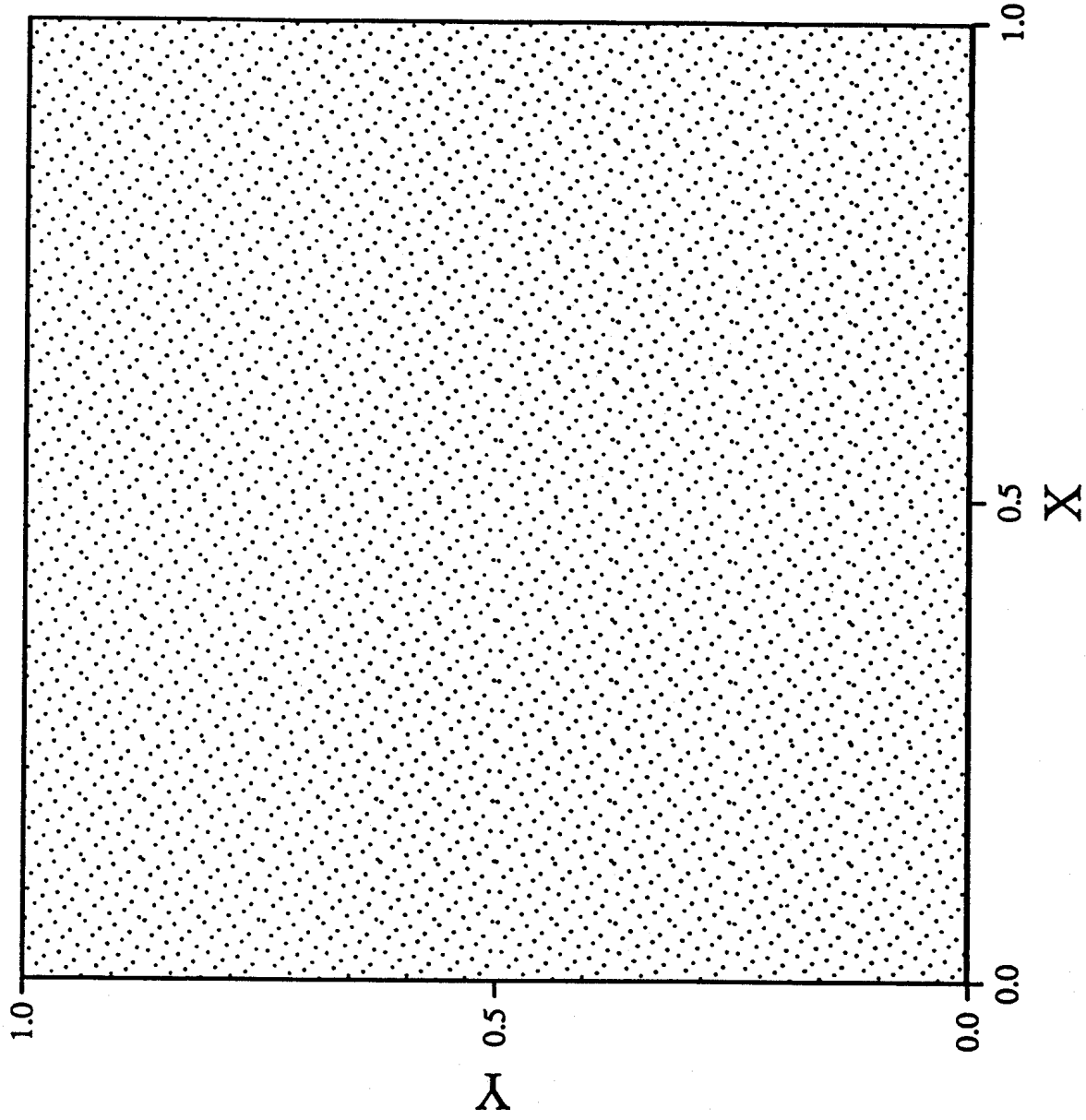

Figure 1b

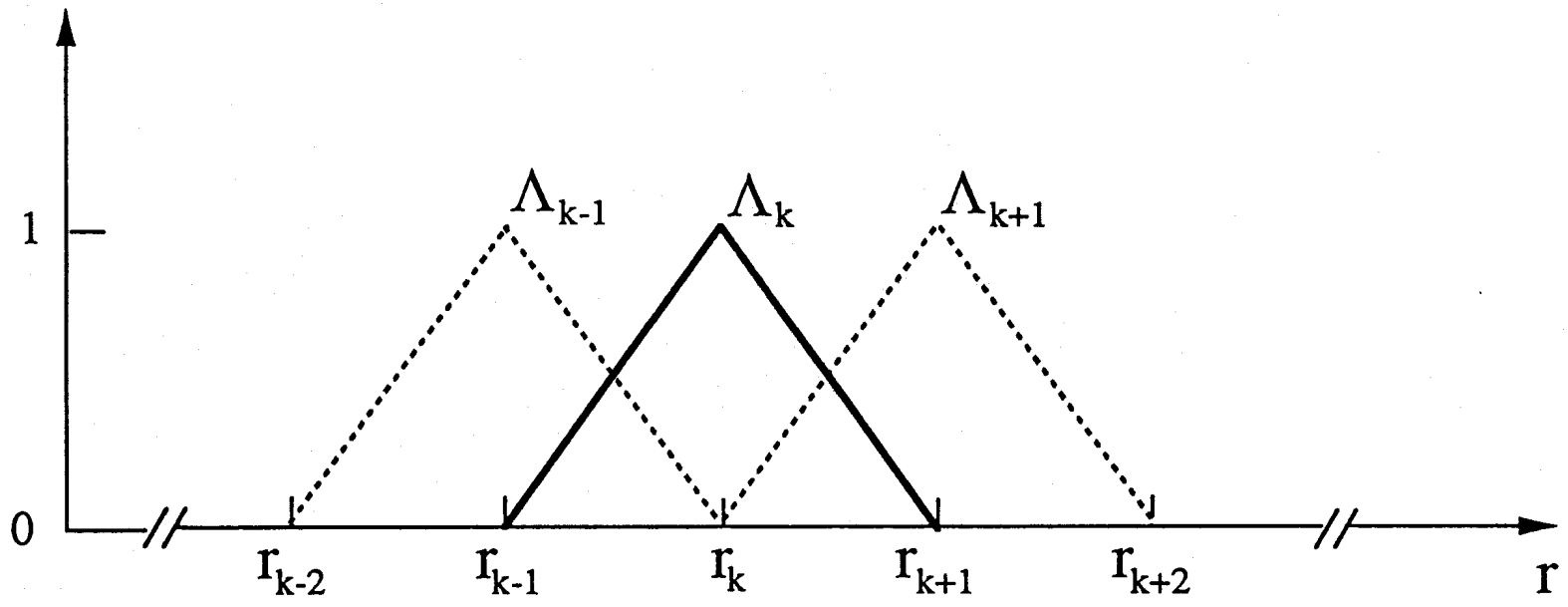

Figure 2